

Entanglement entropy scaling in solid-state spin arrays via capacitance measurements

Leonardo Banchi,¹ Abolfazl Bayat,¹ and Sougato Bose¹

¹*Department of Physics and Astronomy, University College London, Gower Street, WC1E 6BT London, United Kingdom*
(Dated: May 24, 2022)

Solid-state spin arrays are being engineered in varied systems, including gated coupled quantum dots and interacting dopants in semiconductor structures. Beyond quantum computation, these arrays are useful integrated analog simulators for many-body models. As entanglement between individual spins is extremely short ranged in these models, one has to measure the entanglement entropy of a block in order to truly verify their many-body entangled nature. Remarkably, the characteristic scaling of entanglement entropy, predicted by conformal field theory, has never been measured. Here we show that with as few as two replicas of a spin array, and capacitive double-dot singlet-triplet measurements on neighboring spin pairs, the above scaling of the entanglement entropy can be verified. This opens up the controlled simulation of quantum field theories, as we exemplify with uniform chains and Kondo-type impurity models, in engineered solid-state systems. Our procedure remains effective even in the presence of typical imperfections of realistic quantum devices and can be used for thermometry, and to bound entanglement and discord in mixed many-body states.

Introduction.— More than two decades of active research in quantum information processing has promoted various quantum technologies, which are believed to result in a new industrial revolution [1]. One of the major goals, which dates back to Feynmann [2], is to simulate complex interacting quantum systems, which are intractable with classical computers, with an engineered and controllable quantum device, the so-called *quantum simulator* [3]. Unlike general-purpose quantum computers, which are supposed to be programmable to achieve different tasks, quantum simulators are designed for a specific goal, which make them easier to realize. Indeed, so far cold atoms [4] and ions [5] have been used for successfully simulating certain tasks. Nevertheless, solid state based quantum simulator is still highly in demand due to the fact that: i) they provide more versatile types of interaction and stronger couplings compared to cold atoms and ions; ii) the quest towards miniaturization in electronics has reached the quantum level, making solid state quantum devices feasible [6].

Much theoretical researches have been conducted to understand the highly entangled structures appearing in the ground state of quantum many-body systems [7]. For a given bipartition A and B of the whole system, which is assumed to be in the pure state $\rho_{AB} = |\psi_{AB}\rangle\langle\psi_{AB}|$, the *entanglement entropy* is quantified by $S_\alpha(\rho_A) = S_\alpha(\rho_B)$, where $\rho_A = \text{Tr}_B \rho_{AB}$ and S_α is the Renyi entropy, defined as

$$S_\alpha(\rho) = \frac{1}{1-\alpha} \log \text{Tr}[\rho^\alpha], \quad (1)$$

for different values of α . When $\alpha \rightarrow 1$ the Renyi entropy reduces to the von Neumann entropy $S_1(\rho) = -\text{Tr}[\rho \log \rho]$. The importance of the entanglement entropy is twofold: i) it quantifies the entanglement between A and B ; ii) the discovery of its *area law* dependence in non-critical systems has immensely contributed to the development of efficient approximation techniques [8] for describing many-body systems. On the other hand, in critical one-dimensional systems with open boundary conditions, conformal field theory analysis shows that there is a logarithmic correction, as

$$S_\alpha(x) = \frac{c}{12} \left(1 + \frac{1}{\alpha}\right) \log \left[\frac{2N}{\pi} \sin \left(\frac{\pi x}{N} \right) \right] + \kappa_\alpha \quad (2)$$

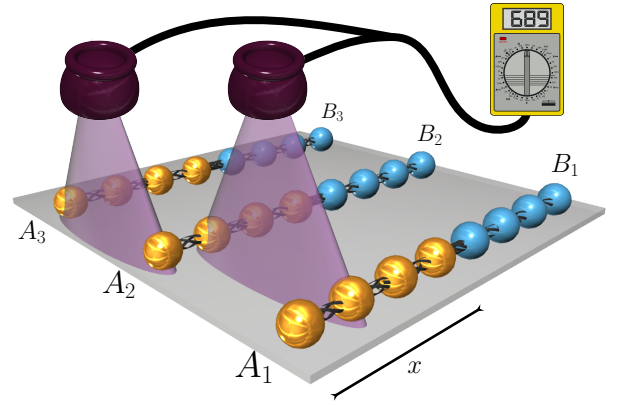


FIG. 1. Scheme for the measurement of the Entanglement entropy for $\alpha=3$ using three copies of the same spin chain. Each spin chain is divided into A_i (yellow spins) and B_i (blue spins). By performing sequential singlet-triplet measurements of pair of spins in neighbouring chains it is possible to estimate $S_{\alpha=3}(\rho_A)$ (see the discussion in the text), which measures the entanglement between A and B .

where x is the size of the contiguous block A starting at one end of system, and N is the total size. When $N \gg x \gg 1$ the usual scaling $S_\alpha \propto \log x$ is obtained. This formula is very general and the *central charge* c only depends on the universality class of the model, while the constants κ_α are model dependent [9–11]. In spite of the extensive theoretical literature on entanglement entropy, its experimental measurement is a big challenge. For itinerant bosonic particles it has been proposed [12, 13], and recently realized [14], to use beam splitter operations or discrete Fourier transform to measure S_α . Alternatively measuring entropy through quantum shot noise has been proposed [15, 16], but not yet realized. On the other hand, in non-itinerant spin systems, the situation become even more difficult and the only proposal so far is to use spin-dependent switches [17], which are difficult to build.

Here we put forward a proposal for measuring S_α in a spin system without demanding time-dependent particle delocalization or spin-dependent switches. While our setup can be realized in different physical systems, we target it to solid state

systems, such as gated quantum dot chains [18–24] or dopant arrays [6, 25–27]. Our procedure is based on well established singlet-triplet measurements, which are now routinely performed either via charge detection [28] or capacitive radio-frequency reflectometry [29–32].

Measuring entanglement entropy.— Our goal is to measure S_α for arbitrarily integer values of $\alpha \geq 2$. For simplicity we explain the procedure for $\alpha=2$ and then generalize it for higher values. Inspired by previous alternative proposals [12, 13, 17, 33, 34] we make use of two copies of a spin array in the state $\rho_1 \otimes \rho_2$ (ideally for perfect copies $\rho_1 = \rho_2$). Each copy is identically divided into two complementary blocks: A_1 and B_1 for the first copy, A_2 and B_2 for the second one (see Fig. 1). Let x be the number of spins in A_1 (and A_2). We define the multi-spin swap operator acting on A_1 and A_2 as

$$P_{12}^A \equiv \bigotimes_{\ell=1}^x \text{SWAP}(\ell_{A_1}, \ell_{A_2}), \quad (3)$$

where $\text{SWAP}(\ell_{A_1}, \ell_{A_2})$ swaps the two spins at the ℓ -th sites in A_1 and A_2 . Since all the operators $\text{SWAP}(\ell_{A_1}, \ell_{A_2})$ are commuting it is simple to show that

$$\langle P_{12}^A \rangle = \text{Tr}[P_{12}^A \rho_1 \otimes \rho_2] = \text{Tr}[\rho_{A_1} \rho_{A_2}] = \text{Tr}[\rho_A^2] \quad (4)$$

where the last equality holds if the two copies are identical, namely $\rho_{A_1} \equiv \rho_{A_2} \equiv \rho_A$. Therefore, Eq. (4) implies that $S_2 = -\log \langle P_{12}^A \rangle$ can be obtained via a sequential measurement of pairwise swap operators acting on the different spins of A_1 and A_2 , as shown in Fig. 1.

The above procedure can be generalized to higher integer values of α by considering α copies of the spin array in the state $\rho^{\otimes \alpha} = \bigotimes_{\ell=1}^{\alpha} \rho_\ell$ (where ideally all the ρ_ℓ 's are equal). Remarkably *sequential* measurements of multi-spin swap operators acting on neighboring copies a and $a+1$, namely $P_{a,a+1}^A$, is sufficient to measure the Renyi entropy. This is simple, but not trivial as better explained in the Appendix A, because some $P_{(a,a+1)}^A$'s for different a are non-commuting. However, we show that the simple sequential measurement, exemplified also in Fig. 1, corresponds to the measurement of the operator $P_{12\dots\alpha}^A$ which is defined recursively by the formula

$$P_{12\dots\alpha}^A = \frac{P_{a,\alpha-1}^A P_{1\dots\alpha-1}^A + P_{1\dots\alpha-1}^A P_{a,\alpha-1}^A}{2}. \quad (5)$$

For example for $\alpha=3$ this reduces to $P_{123}^A = (P_{23}^A P_{12}^A + P_{12}^A P_{23}^A)/2$ and $\langle P_{123}^A \rangle = (\text{Tr}[\rho_{A_1} \rho_{A_2} \rho_{A_3}] + \text{Tr}[\rho_{A_1} \rho_{A_3} \rho_{A_2}])/2$, so that for perfect copies $\langle P_{123}^A \rangle = \text{Tr}[\rho_A^3]$. In general using Eq. (1) we have $S_\alpha(\rho_A) = (1-\alpha)^{-1} \log \langle P_{12\dots\alpha}^A \rangle$. We stress that $P_{12\dots\alpha}^A$ is ultimately written in terms nearest neighbor multi-spin swap operators $P_{(a,a+1)}^A$. This makes the procedure scalable in the lab as one has to first measure P_{12}^A , then P_{23}^A and so forth till $P_{\alpha-1,\alpha}^A$.

Solid state spin chains.— When exactly one electron is trapped in each quantum dot, the interactions between confined electrons in quantum dot arrays is restricted to the spin sector, and is described by the Heisenberg Hamiltonian

$$H = \sum_{k=1}^{N-1} J_k \sigma_k \cdot \sigma_{k+1}, \quad (6)$$

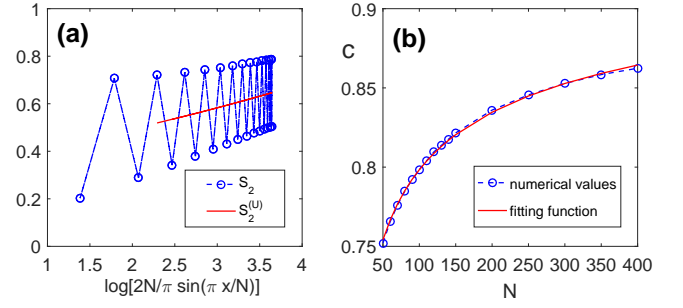


FIG. 2. (color online) (a) Scaling of S_2 and its uniform part $S_2^{(U)}$ in terms of different sizes of block A , for a chain of $N=60$. (b) Scaling of the central charge c as a function of length N .

where J_k is the exchange coupling between neighboring sites and $\sigma_k = (\sigma_k^x, \sigma_k^y, \sigma_k^z)$ is the vector of Pauli operators acting on site k . The couplings J_k can be locally tuned by appropriately changing the local gate voltages. The system can be initialized into its ground state either by cooling, when temperatures is below its energy gap, or using an adiabatic-type evolution [35] when temperature is higher.

Singlet-triplet measurements on two electrons trapped in adjacent quantum dots is now a well-established technique for spin measurements in solid state physics [28, 30–32, 36]. In a quantum mechanical language the singlet-triplet measurements on a pair of electrons in dots a and b correspond to *projective* measurements of the swap operator, as one can show

$$\text{SWAP}(a, b) = \sum_{\mu=\pm,0} |t_\mu\rangle\langle t_\mu| - |s\rangle\langle s| = \frac{\mathbb{1} + \sigma_a \cdot \sigma_b}{2}, \quad (7)$$

$|s\rangle = (|\uparrow_a \downarrow_b\rangle - |\downarrow_a \uparrow_b\rangle)/\sqrt{2}$ is the singlet state, and $|t_+\rangle = |\uparrow_a \uparrow_b\rangle$, $|t_0\rangle = (|\uparrow_a \downarrow_b\rangle + |\downarrow_a \uparrow_b\rangle)/\sqrt{2}$, $|t_-\rangle = |\downarrow_a \downarrow_b\rangle$ are the triplet states. The outcome of this measurement is either $+1$, for triplet outcomes, and -1 for the singlet one.

By comparing Eqs. (7) and (3) it is now clear that, for any given bipartition, we can use a sequence of singlet-triplet measurements to obtain the outcome of the operators $P_{1\dots\alpha}^A$ and thus compute all the Renyi entropies S_α for all integer $\alpha \geq 2$. As described before, and shown also in Fig. 1, the total number of singlet-triplet measurements to be performed for a single outcome is $x\alpha$ where x is the number of spins in subsystem A . To measure $P_{1\dots\alpha}^A$ we first switch off the J_k 's within each array, and then lower the barriers between pairs of spins in two different arrays to perform the singlet-triplet measurements. A recently developed multiplexer structure [37] containing two parallel arrays of quantum dots is a promising setup, which can be adapted for measuring S_2 with our proposed mechanism. Motivated by this operating device, and for the sake of simplicity, in the rest of the paper we focus on $\alpha=2$. Numerical results are obtained with either Density Matrix Renormalization Group (DMRG) or exact diagonalization for short chains.

Application 1: conformal field theory in the lab.— We first present how field theory predictions, given in Eq. (2), can be verified for a uniform chain where $J_k = J$, for all k 's. In the thermodynamic limit $N \rightarrow \infty$ it is known that the central charge

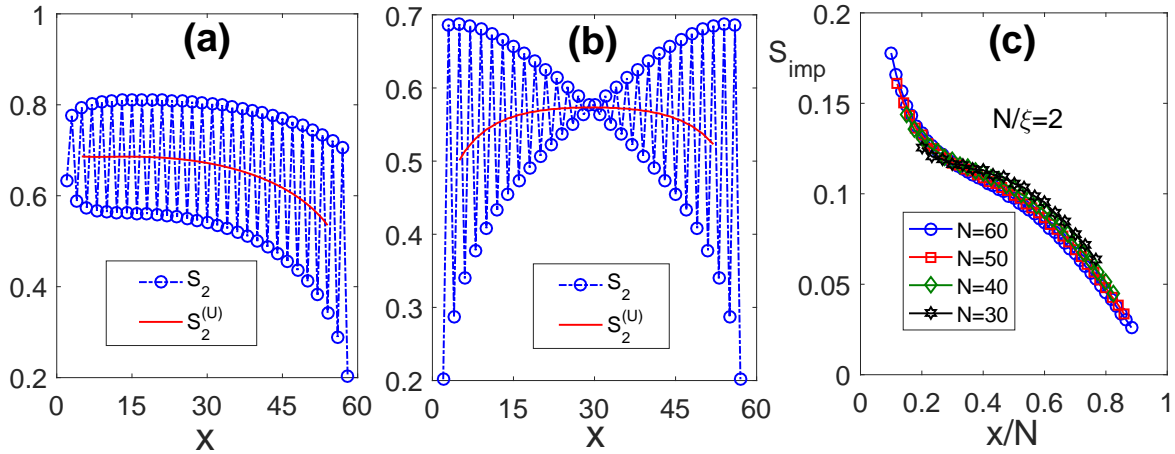


FIG. 3. (color online) (a) The Renyi entropy $S_2(x, N, \xi)$ and its uniform part $S_2^{(U)}$ in a chain of length $N=60$. (b) The bulk Renyi entropy $S_2(x-1, N-1)$ and its uniform part $S_2^{(U)}(x-1, N-1)$ in a homogeneous chain of 59 sites without impurity. (c) Data collapse for different chains when J' is tuned to keep $N/\xi=2$.

is $c=1$. In Fig. 2(a) we plot the Renyi entropy S_2 as a function of $\log[\frac{2N}{\pi} \sin(\frac{\pi x}{N})]$ in a chain of length $N=60$. For open boundary conditions, finite size effects are known [9] to give rise to an alternating behaviour of $S_2(x) = S_2^{(U)} + (-1)^x S_2^{(A)}$. Using the methodology of Ref. [38] we extract the uniform part $S_2^{(U)}$, which is dominant for $N \rightarrow \infty$ and follows the scaling of (2). In Fig. 2(a) we also plot $S_2^{(U)}$ in red colors, showing perfect linear scaling. From the slope of this line we can extract the central charge c , which asymptotically approaches its thermodynamic limit value, $c=1$. This can be seen in Fig. 2(b) where we also plot the fitting function $c = 1 - 0.7536N^{-0.2848}$. Such slow convergence is due to finite-size corrections to the field theory predictions [39], which here, for simplicity, we have absorbed into the definition of c .

Application 2: impurity entanglement entropy.— Introducing one or more impurities in the system can change its behaviour dramatically. A paradigmatic example is the single-impurity Kondo model [40] in which a single impurity in a gapless system creates a length scale ξ , known as Kondo length. The scaling features of Kondo physics can be captured by a spin chain emulation of this model [38]. This is described by Eq. (6) where $J_1=J'$ while all other couplings remain uniform $J_k=J$ (for $k \geq 2$). Moreover, the length scale is determined by J' as $\xi \propto e^{g/J'}$ for some constant g . The presence of the impurity modifies the scaling of the Eq. (2) when $x < \xi$. In order to capture the impurity contribution of the entanglement entropy we extend the ansatz of Ref. [38] for S_1 to generic S_α and define the impurity entanglement entropy as

$$S_\alpha^{(imp)}(x, N, \xi) = S_\alpha^{(U)}(x, N, \xi) - S_\alpha^{(U)}(x-1, N-1), \quad (8)$$

where $S_\alpha^{(U)}(x, N, \xi)$ is the Renyi entropy of a block of size x in a chain of length N and impurity coupling J' , which determines ξ , while $S_\alpha^{(U)}(x-1, N-1)$ represents the bulk contribution of the uniform chain when the impurity is removed. In Fig. 3(a) we plot the $S_2(x, N, \xi)$ and its uniform part $S_2^{(U)}$ in a

chain of length $N=60$. The bulk contribution of the uniform chain, i.e. $S_2(x-1, N-1)$, and its uniform part $S_2^{(U)}(x-1, N-1)$ are plotted in Fig. 3(b). The qualitative difference between Fig. 3(a) and Fig. 3(b) is due to the different parities (i.e. even and odd) of the chains.

The emergence of the length scale implies that $S_2^{(imp)}(x, N, \xi)$ is only a function of the ratios $S_2^{(imp)}(x/N, N/\xi)$. To verify this scaling we fix N/ξ and plot $S_2^{(imp)}$ as a function of x/N for different lengths N . To keep N/ξ fixed J' has to be tuned according to Ref. [41]. The results are shown in Fig. 3(c) where, as predicted, the curves of different chains collapse on each other. Although the data collapse becomes better by increasing the system size, Fig. 3(c) shows that the scaling predictions can be captured even in relatively small chains.

Application 3: entanglement spectrum.— For any pure state ρ_{AB} the eigenvalues of ρ_A are called *entanglement spectrum* [42], whose analysis is important to characterize quantum phase transitions [43, 44]. The eigenvalues of ρ_A are the roots of $q(\lambda) = \det(\lambda \mathbb{1} - \rho_A)$, which can be written as $q(\lambda) = \sum_k g_k \lambda^k$. According to Ref. [45] the coefficients g_k can be obtained algorithmically from $\text{Tr}[\rho_A^\alpha]$ for $\alpha=1, \dots, k$. Since these traces can be measured with our procedure one can build $q(\lambda)$ and hence obtain the full entanglement spectrum. Clearly, given a maximum number of copies α_{\max} , one can find the entanglement spectrum for block sizes as large as $x = \log_2 \alpha_{\max}$.

Application 4: thermometry via purity measurement.— One of the biggest challenges in solid-state experiments is to measure the *true* temperature of electrons, as it is normally higher than the temperature of the refrigerator. Remarkably, our scheme enables also to measure the electronic temperature via singlet-triplet measurements, assuming that the system is in a thermal state $\rho_\beta = e^{-\beta H}/Z$. Our approach is based on three distinctive features of engineered solid state structures: i) the exchange integral J can be varied; ii) the purity $\mathcal{P}(\beta, J) = \text{Tr}[\rho_\beta^2] = e^{-S_2(\rho_\beta)}$ can be measured with our scheme by

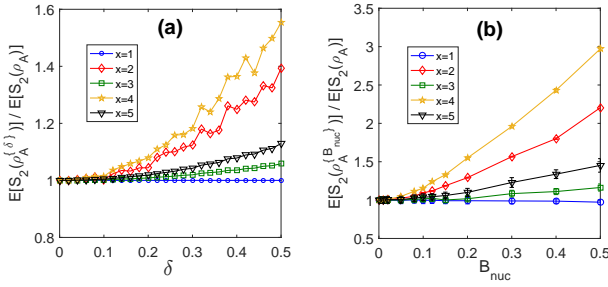


FIG. 4. (color online) (a) Average $\mathbb{E}[S_2(\rho_A^{[\delta]})]$ over 1000 random sets of couplings $J_k^{(j)} = J_k(1 + \epsilon_k^{(j)})$, where $j=1, 2$ refers to the different copies, $J_k=J$ and $\epsilon_k^{(j)}$ is uniformly distributed in $[-\delta, +\delta]$ for different block sizes x (b) Monte Carlo simulation of $\mathbb{E}[S_2(\rho_A^{B_{\text{nuc}}})]$ for the effect of random fields $B_k^{(j)}$ as a function of the strength of the hyperfine interaction B_{nuc} . In both figures the entropies are normalized with respect to the error-free case $S_2(\rho_A)$, and $N=10$.

taking two copies and $x=N$; iii) computing the energy expectation $E(\beta, J) = \text{Tr}[H\rho_\beta]$ is reduced to singlet-triplet measurements on neighboring sites of one of the arrays, thanks to Eqs. (7) and (6). A simple calculation reveals that $\frac{\partial \mathcal{P}(\beta, J)}{\partial J} = \frac{\beta}{J} [2E(\beta, J) - E(\beta, 2J)] \mathcal{P}(\beta, J)$. Aside from β all the quantities in the above equality can be measured either directly (namely $\mathcal{P}(\beta, J)$ and $E(\beta, J)$) or through the variation of J (namely $\frac{\partial \mathcal{P}(\beta, J)}{\partial J}$ and $E(\beta, 2J)$). In summary, thanks to the above equality, using different singlet-triplet measurements with different values of J it is possible to infer β and thus the temperature.

Application 5: bounding entanglement and discord in mixed states.— The Renyi entropy of a block A is a measure of entanglement between A and B only if ρ_{AB} is a pure state. However, we show that it is still possible to bound the amount of entanglement and discord also for mixed states by measuring both $S_\alpha(\rho_A)$ and $S_\alpha(\rho_{AB})$. The distillable entanglement E_D , an operational entanglement measure, satisfies the *hashing inequality* [46], $E_D \geq \max_{X=A,B} I_1(X)$, where $I_1(X) = S_1(\rho_X) - S_1(\rho_{AB})$. Similarly, for the quantum discord $D(A|B)$, which is an asymmetric measure of quantum correlations between A and B [47], it is known that $D(A|B) \geq I_1(A)$ and similarly $D(B|A) \geq I_1(B)$ [48]. The von Neumann entropy S_1 can be extrapolated [49] from S_α for different integers $\alpha \geq 2$, which can be measured with our scheme. However, we show that I_1 can also be bounded by directly measuring $S_2(\rho_A)$ and $S_2(\rho_{AB})$, which require only two replicas. Indeed, since $S_2(\rho) \leq S_1(\rho) \leq f[S_2(\rho)]$, where f is given in Ref. [50], we obtain $I_1(X) \geq I_2(X)$ where $I_2(X) = S_2(\rho_X) - f[S_2(\rho_{AB})]$. For either $X=A, B$, $I_2(X)$ thus provides a measurable lower bound to entanglement and discord.

Imperfections.— Realistic experimental imperfections may introduce errors, e.g. by making the different copies non-identical. Our protocol provides $\text{Tr}[\rho_{A_1} \rho_{A_2}]$, as given in Eq. (4), which may deviate from the ideal case $\text{Tr}[\rho_A^2]$. Indeed, imperfect fabrication may result in random couplings $J_k^{(j)} \rightarrow J_k(1 + \epsilon_k^{(j)})$, where j is the index of different copies and $\epsilon_k^{(j)}$ is a random number uniformly distributed between

$[-\delta, +\delta]$. In Fig.4(a) we calculate the average $\mathbb{E}[S_2(\rho_A^{[\delta]})]$ over 1000 random sets of couplings for different block sizes x , normalized with respect to its value at $\delta=0$. As the figure shows the average entropy increases by increasing δ . Moreover, up to $\delta=10\%$ the outcomes are almost indistinguishable from the error-free case.

The second source of imperfections is due to the hyperfine interaction with the nuclear spins in the bulk, which effectively introduces an extra term $\sum_k \mathbf{B}_k^{(j)} \cdot \boldsymbol{\sigma}_k$ in the Hamiltonian (6), where each component of the random fields has a normal distribution with zero mean and variance B_{nuc} . Unlike the randomness in the couplings, which is constant over different experiments being due to the fabrication, the effective random fields are different in any experimental repetition. To realistically model this, we perform a Monte Carlo simulation of real experimental outcomes (see the Appendix C for details). The results are shown in Fig. 4(b) for different block sizes x . For realistic values of $B_{\text{nuc}}=0.1J$ [28] we see that the entanglement entropy is only slightly affected by hyperfine interactions. The increasing trend of the entropy as a function of the noise, which is consistent with Ref. [51], is further discussed in the Appendix B.

Conclusions.— We propose a scheme to experimentally measure the entanglement between blocks in engineered solid state quantum devices. Our procedure is based on singlet-triplet measurements which are routinely performed in quantum dot systems. All the Renyi entanglement entropies S_α for integer $\alpha \geq 2$ can be measured via α replicas of the system. Although for uniform chains the convergence of the central charge is slow, the logarithmic scaling predictions can already be verified with reasonably small system sizes ($\lesssim 60$). Moreover, in the Kondo impurity model we found that the impurity contribution in the Renyi entropy satisfies a universal scaling law. Despite the fact this law has been obtained in the thermodynamic limit, remarkably it can be observed for chains as small as $N \gtrsim 30$. In addition, our scheme enables the measurement of the purity of the whole system, which allows one to measure the true temperature of electrons in a thermal state. Our procedure remains effective even in the presence of typical imperfections due to imperfect fabrication and hyperfine interactions. Although our scheme has been targeted to quantum dot arrays, the same protocol can also be realized in other systems, such as dopants in silicon [26].

ACKNOWLEDGMENTS

Acknowledgements.— LB and SB have received funding from the European Research Council under the European Unions Seventh Framework Programme (FP/2007-2013) / ERC Grant Agreement No. 308253. AB and SB acknowledge the EPSRC grant EP/K004077/1.

Appendix A: Renyi entropies of arbitrary orders via singlet-triplet measurements

Singlet-triplet (ST) projective measurements can be described by the pair of projection operators $\Pi_- = |s\rangle\langle s|$, $\Pi_+ = \sum_{\alpha=-1}^1 |t_\alpha\rangle\langle t_\alpha|$ where $|s\rangle = (|\uparrow\downarrow\rangle - |\downarrow\uparrow\rangle) / \sqrt{2}$ is the singlet state, and $|t_1\rangle = |\uparrow\uparrow\rangle$, $|t_0\rangle = (|\uparrow\downarrow\rangle + |\downarrow\uparrow\rangle) / \sqrt{2}$, $|t_{-1}\rangle = |\downarrow\downarrow\rangle$ are the triplet states. To relate this measurement with the estimation of the entropy it is convenient to define the swap operator SWAP which is related to the ST-measurement via $\Pi_\pm = (\mathbb{1} \pm \text{SWAP})/2$. Note that the SWAP operator can be also written in terms of the Heisenberg spin exchange $\text{SWAP} = (\mathbb{1} + \sum_{\alpha=x,y,z} \sigma_\alpha \otimes \sigma_\alpha) / 2$, where σ_α are the Pauli matrices. Since $\text{SWAP} = \Pi_+ - \Pi_-$ the ST-measurement can be understood as a projective measurement of the SWAP operator: given a two qubit state, this measurement can result in two different outcomes, either +1 or -1, with respective probability $\text{Tr}[\rho \Pi_\pm]$.

Our strategy to measure the Renyi entropy $S_\alpha(\rho) = (1-\alpha)^{-1} \log \text{Tr}[\rho^\alpha]$, is based on two fundamental observations: (i) as shown in [33] if one has access to m copies of the *same* state ρ , then $\text{Tr}[\rho^m] = \text{Tr}[P_{(12\dots m)} \rho^{\otimes m}]$ where $\rho^{\otimes m} = \rho \otimes \rho \otimes \dots \otimes \rho$ and $P_{(12\dots m)} |\psi_1\rangle \otimes |\psi_2\rangle \dots |\psi_m\rangle = |\psi_m\rangle \otimes |\psi_1\rangle \dots |\psi_{m-1}\rangle$ is a permutation operator, which swaps different states according to the *cyclic* permutation $(12\dots m)$; (ii) the operator $P_{(12\dots m)}$ can be decomposed in terms of a series of swap between neighboring copies. In the following we show how to interpret these multiple swap operations in terms of single-triplet measurements, as shown in Fig. 1.

We first focus on the measure of the entanglement entropy for $\alpha=2$. This is quite straightforward, but we review this in detail to introduce the necessary formalism and to clarify why this simple analysis cannot be applied for $\alpha>2$. We consider two copies of the same system, each divided into two disjoint blocks: the first copy is composed by the blocks A_1 and B_1 and the second one by the blocks A_2 and B_2 . From the previous analysis it is clear that $S_2 = \frac{1}{2} \log \langle P_{(12)}^A \rangle$, where $P_{(12)}^A$ is a multi-spin swap between the spins in A_1 and those in A_2 . Let x be the number of spins in A_1 (and A_2) and let $i_1 \dots i_x$ be the indices of the spin in A_1 , while $j_1 \dots j_x$ are the indices of the spins in A_2 . Blocks A_1 and A_2 are non-overlapping. The multi-spin swap then reads $P_{(12)}^A \equiv \bigotimes_{\ell=1}^x \text{SWAP}_{i_\ell j_\ell}$ where SWAP_{ij} is the swap operator between the pair of spins (i, j) . Therefore, in order to measure the expectation value $\langle P_{(12)}^A \rangle$, one has to perform a series of multiple singlet-triplet measurements between different pairs (i_ℓ, j_ℓ) of spins, and collect the resulting statistics. Indeed, the first projective measurement will result in an outcome ± 1 and a collapse of $\rho_{A_1 A_2 B_1 B_2}$ into the (non-normalized) state $\Pi_\pm^{(i_1, j_1)} \rho_{A_1 A_2 B_1 B_2} \Pi_\pm^{(i_1, j_1)}$, where $\Pi_\pm^{(i_1, j_1)}$ is the ST projector for the pair (i_1, j_1) ; after the x projective measurements between all pair of spins the outcome will be $(\prod_{\ell=1}^x \beta_\ell) \mathbb{1}$, where $\beta_\ell = \pm 1$, with probability $\text{Tr}[\rho_{A_1 A_2 B_1 B_2} \bigotimes_{\ell=1}^x \Pi_{\beta_\ell}^{(i_\ell, j_\ell)}]$. Therefore, running these projections many-times will enable an experimental evaluation of $\langle P_{(12)}^A \rangle$.

We now consider the case $\alpha=3$. For convenience we write $P_{(12)}^A = \Pi_{(12)}^+ - \Pi_{(12)}^-$ in terms of the projection operators (indeed,

as shown before also $P_{(12)}^A$ has eigenvalues ± 1). We first perform a sequential set of ST-measurements on copies $(1, 2)$, with outcome β_1 and then do the same measurement on copies $(2, 3)$, with outcome β_2 . We introduce the notation $P_{(23)}^A \circ P_{(12)}^A$ to describe this process. After the first measurement, the (non-normalized) state of the system will be $\Pi_{(12)}^{\beta_1} \rho \Pi_{(12)}^{\beta_1}$, where $\rho = \rho_1 \otimes \rho_2 \otimes \rho_3$, while after the two sets of measurements it is $\Pi_{(23)}^{\beta_2} \Pi_{(12)}^{\beta_1} \rho \Pi_{(12)}^{\beta_1} \Pi_{(23)}^{\beta_2}$. Therefore,

$$\begin{aligned} \langle P_{(23)}^A \circ P_{(12)}^A \rangle &= \sum_{\beta_2} \sum_{\beta_1} \beta_1 \beta_2 \text{Tr} \left[\Pi_{(23)}^{\beta_2} \Pi_{(12)}^{\beta_1} \rho \Pi_{(12)}^{\beta_1} \Pi_{(23)}^{\beta_2} \right] \\ &= \sum_{\beta_2} \sum_{\beta_1} \beta_1 \beta_2 \text{Tr} \left[\Pi_{(12)}^{\beta_1} \Pi_{(23)}^{\beta_2} \Pi_{(12)}^{\beta_1} \rho \right] \\ &= \sum_{\beta_1} \beta_1 \text{Tr} \left[\Pi_{(12)}^{\beta_1} P_{(23)}^A \Pi_{(12)}^{\beta_1} \rho \right] \\ &= \frac{1}{2} \left(\text{Tr} [P_{(12)}^A P_{(23)}^A \rho] + \text{Tr} [P_{(23)}^A P_{(12)}^A \rho] \right) \\ &= \frac{1}{2} \left(\text{Tr} [P_{(123)}^A \rho] + \text{Tr} [P_{(132)}^A \rho] \right) \\ &= \frac{1}{2} \left(\text{Tr} [\rho_1 \rho_2 \rho_3] + \text{Tr} [\rho_1 \rho_3 \rho_2] \right), \end{aligned} \quad (\text{A1})$$

where we used multiple times the fact that $\Pi_{(ab)}^\pm = (\mathbb{1} \pm P_{(ab)}^A) / 2$ and, in the last equation, that $P_{(123)}^A$ and $P_{(132)}^A$ are permutation operators, and $(123), (132)$ different cycles. The above equation shows that, because of the non-commutative nature of $P_{(12)}^A$ and $P_{(23)}^A$, the sequential process described in Fig. 1 ends up in the measurement of a combination of different permutation operators.

We now generalize the above argument for higher values of α . We apply sequential ST-measurements on neighbouring copies, using the notation $P_{(12)}^A \circ P_{(23)}^A \circ \dots \circ P_{(\alpha-1, \alpha)}^A$, meaning that we first perform $P_{(12)}^A$ and so forth. As already seen for $\alpha=3$, the reason for this notation is that, as we show, $\langle P_{(12)}^A \circ P_{(23)}^A \circ \dots \circ P_{(\alpha-1, \alpha)}^A \rangle \neq \langle P_{(12)}^A P_{(23)}^A \dots P_{(\alpha-1, \alpha)}^A \rangle$. Indeed, after the first measurement of $P_{(12)}^A$, with outcome $\beta_1 = \pm 1$, the (non-normalized) state is $\Pi_{(12)}^{\beta_1} \rho_{AB} \Pi_{(12)}^{\beta_1}$. At later stages one performs sequentially the other measurements $P_{(j, j+1)}^A$, getting the outcomes β_j . Taking the averages one then finds that

$$\langle P_{(\alpha-1, \alpha)}^A \circ \dots \circ P_{(12)}^A \rangle = \text{Tr} [\mathcal{P}_{\alpha-1, \alpha} [\dots \mathcal{P}_{23} [\mathcal{P}_{12} [\rho]]] \dots],$$

where $\mathcal{P}_{j, j+1}[\rho] = \sum_{\beta_j} \beta_j \Pi_{(j, j+1)}^{\beta_j} \rho \Pi_{(j, j+1)}^{\beta_j}$. Using the cyclic property of the trace and the identity $\mathcal{P}_{j-1, j} [P_{(nab\dots)}^A] = [P_{(j-1, j, a, \dots)}^A + P_{(j, j-1, a, \dots)}^A] / 2$ multiple times (where $a > j$, $b > j$ and so forth), one finds that $\langle P_{(\alpha-1, \alpha)}^A \circ \dots \circ P_{(12)}^A \rangle = 2^{2-\alpha} \sum_c \langle P_c^A \rangle$ where c are $2^{\alpha-2}$ different *cycles*, namely cyclic permutations of the elements $1, \dots, \alpha$. For instance, for $\alpha=3$ one has $c = \{(123), (132)\}$. From the above expression it turns out that, if the copies are perfect, then the different cycles have the same expectation value $\langle P_c^A \rangle = \text{Tr}[\rho^\alpha]$ and therefore

$$S_\alpha = \frac{1}{1-\alpha} \log \langle P_{(\alpha-1, \alpha)}^A \circ \dots \circ P_{(12)}^A \rangle. \quad (\text{A2})$$

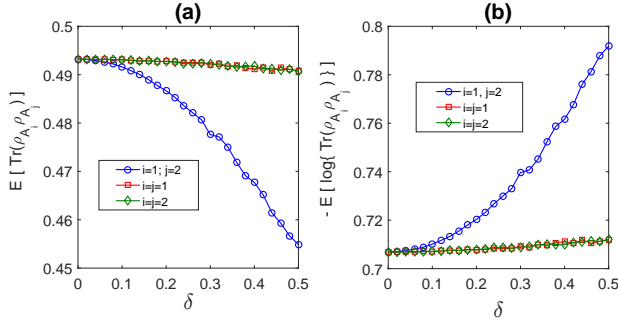


FIG. 5. (a) Average purity $\mathbb{E}[\text{Tr}[\rho_{A_i}\rho_{A_j}]]$ and (b) average Renyi entropy $\mathbb{E}[-\log \text{Tr}[\rho_{A_i}\rho_{A_j}]]$ as a function of the noise strength δ , calculated with our strategy (where $i \neq j$ and each copy feels a different noise) and with the standard procedure (where $i = j$). In all cases $N=10$, $x=5$.

On the other hand, if the different copies are not exactly equal, then there may be an extra error (see the numerical examples in the main text). In Eq.(A2) each $P_{(j,j+1)}^A$ requires x ST-measurements (x being the number of spins in A_i), so the total number of ST-measurements for a single outcome is $x\alpha$.

Appendix B: Imperfections

We compare the role of the imperfections in our protocol and in the standard one in Fig. 5. We consider the noise model discussed in the main text where the couplings J_k are different over the different copies, namely $J_k^{(j)} = J_k(1 + \epsilon_k^{(j)})$ where j refers to the index of the copies. The errors $\epsilon_k^{(j)}$ are independent identically distributed according to a uniform distribution with zero mean and variance δ . For simplicity we consider only $\alpha=2$. In Fig. 5(a) we show that the average purity estimated with our strategy, i.e. $\mathbb{E}[\text{Tr}[\rho_{A_1}\rho_{A_2}]]$, is smaller than the one evaluated with the standard procedure on each chain, i.e. $\mathbb{E}[\text{Tr}[\rho_{A_1}^2]]$ and $\mathbb{E}[\text{Tr}[\rho_{A_2}^2]]$. On the other hand, since the Renyi entropy is minus the logarithm of the purity, the average Renyi entropy displays the opposite behavior, as shown in Fig. 5(b). This can be explained with the following argument. When $\epsilon_k^{(j)} \ll 1$ we can expand the states ρ_{A_j} in series of $\epsilon_k^{(j)}$ and write

$$\rho_{A_j} \approx \rho_A + \sum_k \epsilon_k^{(j)} \rho'_k + \sum_{k,\ell} \epsilon_k^{(j)} \epsilon_\ell^{(j)} \rho''_{k,\ell}, \quad (\text{B1})$$

where ρ'_k and $\rho''_{k,\ell}$ are the first order and second-order expansion, which are independent on the index j . Therefore,

$$\mathbb{E}[\text{Tr}[\rho_{A_1}\rho_{A_2}]] \approx \text{Tr}[\rho_A^2] + 2\delta^2 \sum_k \text{Tr}[\rho''_{k,k}\rho_A], \quad (\text{B2})$$

while

$$\begin{aligned} \mathbb{E}[\text{Tr}[\rho_{A_1}^2]] &= \mathbb{E}[\text{Tr}[\rho_{A_2}^2]] \\ &\approx \text{Tr}[\rho_A^2] + \delta^2 \sum_k (2 \text{Tr}[\rho''_{k,k}\rho_A] + \text{Tr}[\rho_k'^2]). \end{aligned} \quad (\text{B3})$$

The results of Fig. 5 show that the quantity $\sum_k \text{Tr}[\rho''_{k,k}\rho_A]$ is negative and lowers the average purity. On the other hand, $\text{Tr}[\rho_k'^2]$ is clearly positive, being the trace of the square of an operator. The latter term then partially removes the effect of the negative one and makes $\mathbb{E}[\text{Tr}[\rho_{A_i}^2]] \approx \text{Tr}[\rho_A^2]$. On the other hand, independent copies are slightly more affected by the uncorrelated noise and $\mathbb{E}[\text{Tr}[\rho_{A_1}\rho_{A_2}]] < \mathbb{E}[\text{Tr}[\rho_{A_i}^2]] \leq \text{Tr}[\rho_A^2]$. The error is nonetheless small, since it is smaller than 10% even for 50% of randomness.

Appendix C: Monte Carlo simulation of random fields

As explained in the main text, hyperfine interactions with the nuclear spins result in the couplings $\sum_k \mathbf{B}_k \cdot \boldsymbol{\sigma}$. The random effective fields \mathbf{B}_k are assumed to be constant after each different ST-measurement required to get a single outcome. However, to get the necessary statistics to estimate (A2) one has to repeat the experiment many times. Since each time the system is re-initialized, the corresponding random fields may be different. To study this kind of imperfections we perform the following Monte Carlo simulation

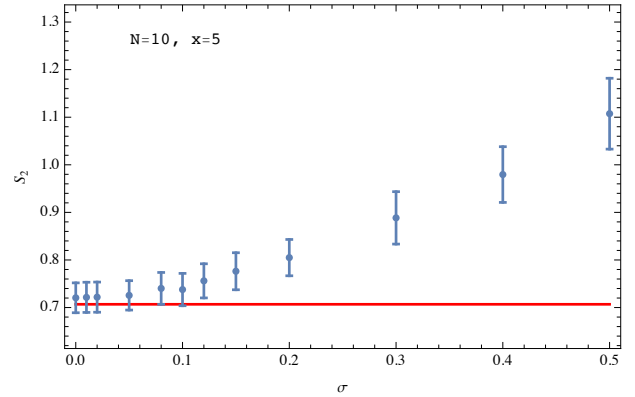
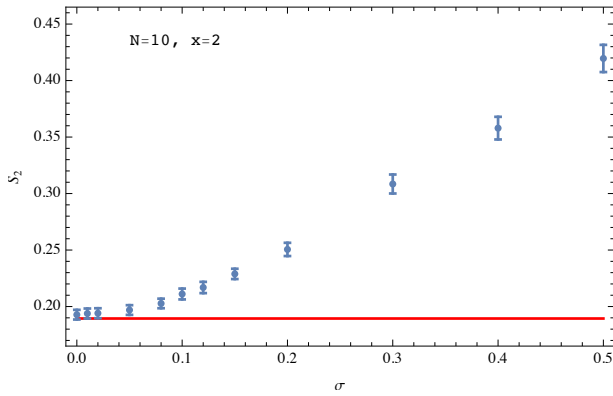
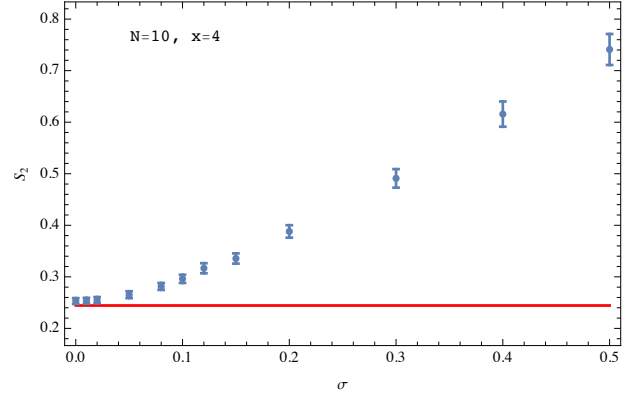
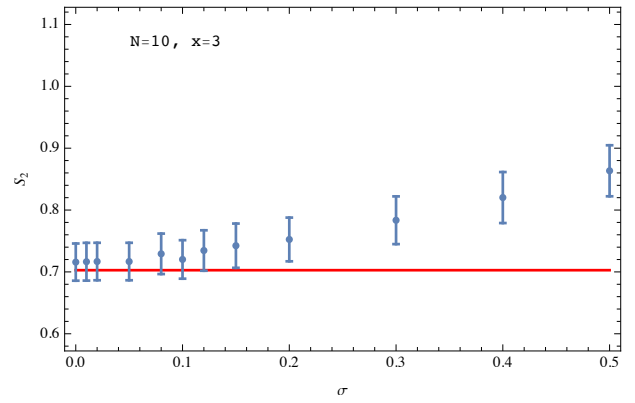
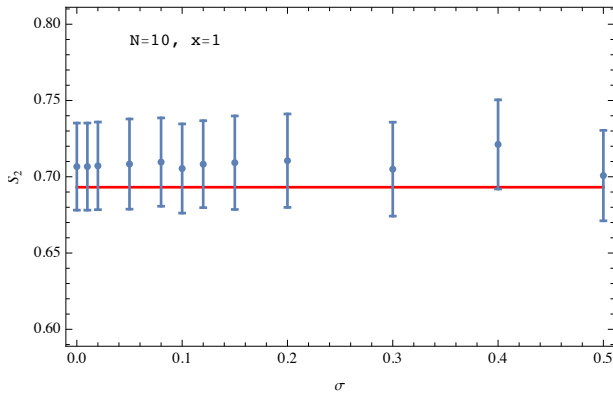
1. We generate the random fields $B_{k,c}^\alpha$ for different $\alpha=x,y,z$, different sites $k=1, \dots, N$ and different copies $c=1, \dots, \alpha$ independently according to a Gaussian distribution, with zero mean and variance σ .
2. We calculate, with exact numerical diagonalization, the quantum mechanical probability

$$p = \sum_{\prod_j \beta_j = +1} \text{Tr} \left[\prod_j \Pi_{(j,j+1)}^{\beta_j} \rho \prod_l \Pi_{(l,l+1)}^{\beta_l} \right],$$

to get the outcome $+1$. In the above equation $\rho = \rho_1 \otimes \dots \otimes \rho_\alpha$ where ρ_j is the ground state of the j -th copy with the random fields. In general therefore $\rho_i \neq \rho_j$.

3. We generate a random number q in $[0, 1]$. If $q < p$ we say that the outcome of the sequence of projective measurements is $+1$, otherwise it is -1 .
4. We repeat the steps 1,2,3 T times to estimate $\langle P_{(\alpha-1,\alpha)}^A \circ \dots \circ P_{(1,2)}^A \rangle$, and then calculate S_α .
5. We repeat the steps 1,2,3,4 K times to calculate the average $\mathbb{E}[S_\alpha]$ and the variance.

In the following figures we show the outcome of this procedure for $N=10$, $x=1, \dots, N/2$ as a function of σ , when $K=T=100$. The red lines correspond to the exact numerical calculation of S_α when $\sigma=0$.



-
- [1] J. P. Dowling and G. J. Milburn, *Philosophical Transactions of the Royal Society of London A: Mathematical, Physical and Engineering Sciences* **361**, 1655 (2003).
- [2] R. P. Feynman, *International journal of theoretical physics* **21**, 467 (1982).
- [3] J. I. Cirac and P. Zoller, *Nature Physics* **8**, 264 (2012).
- [4] I. Bloch, J. Dalibard, and S. Nascimbene, *Nature Physics* **8**, 267 (2012).
- [5] R. Blatt and C. Roos, *Nature Physics* **8**, 277 (2012).
- [6] J. Salfi, J. Mol, R. Rahman, G. Klimeck, M. Simmons, L. Hollenberg, and S. Rogge, *Nature communications* **7** (2016).
- [7] L. Amico, R. Fazio, A. Osterloh, and V. Vedral, *Reviews of Modern Physics* **80**, 517 (2008).
- [8] J. Eisert, M. Cramer, and M. B. Plenio, *Reviews of Modern Physics* **82**, 277 (2010).
- [9] P. Calabrese, M. Campostrini, F. Essler, and B. Nienhuis, *Physical review letters* **104**, 095701 (2010).
- [10] P. Calabrese and J. Cardy, *Journal of Statistical Mechanics: Theory and Experiment* **2004**, P06002 (2004).
- [11] M. Fagotti and P. Calabrese, *Journal of Statistical Mechanics: Theory and Experiment* **2011**, P01017 (2011).
- [12] C. M. Alves and D. Jaksch, *Physical review letters* **93**, 110501 (2004).
- [13] A. Daley, H. Pichler, J. Schachenmayer, and P. Zoller, *Physical review letters* **109**, 020505 (2012).
- [14] A. M. Kaufman, M. E. Tai, A. Lukin, M. Rispoli, R. Schittko, P. M. Preiss, and M. Greiner, *arXiv preprint arXiv:1603.04409* (2016).
- [15] H. F. Song, S. Rachel, C. Flindt, I. Klich, N. Laflorencie, and K. Le Hur, *Physical Review B* **85**, 035409 (2012).

- [16] I. Klich and L. Levitov, *Physical review letters* **102**, 100502 (2009).
- [17] D. A. Abanin and E. Demler, *Physical review letters* **109**, 020504 (2012).
- [18] D. Loss and D. P. DiVincenzo, *Physical Review A* **57**, 120 (1998).
- [19] R. Hanson, L. Kouwenhoven, J. Petta, S. Tarucha, and L. Vandersypen, *Reviews of Modern Physics* **79**, 1217 (2007).
- [20] T. Baart, N. Jovanovic, C. Reichl, W. Wegscheider, and L. Vandersypen, arXiv preprint arXiv:1606.00292 (2016).
- [21] T. Nakajima, M. R. Delbecq, T. Otsuka, S. Amaha, J. Yoneda, A. Noiri, K. Takeda, G. Allison, A. Ludwig, A. D. Wieck, *et al.*, arXiv preprint arXiv:1604.02232 (2016).
- [22] T. Ito, T. Otsuka, S. Amaha, M. R. Delbecq, T. Nakajima, J. Yoneda, K. Takeda, G. Allison, A. Noiri, K. Kawasaki, *et al.*, arXiv preprint arXiv:1604.04426 (2016).
- [23] D. Zajac, T. Hazard, X. Mi, E. Nielsen, and J. Petta, arXiv preprint arXiv:1607.07025 (2016).
- [24] A. Noiri, J. Yoneda, T. Nakajima, T. Otsuka, M. R. Delbecq, K. Takeda, S. Amaha, G. Allison, A. Ludwig, A. D. Wieck, *et al.*, *Applied Physics Letters* **108**, 153101 (2016).
- [25] B. E. Kane, *nature* **393**, 133 (1998).
- [26] F. A. Zwanenburg, A. S. Dzurak, A. Morello, M. Y. Simmons, L. C. Hollenberg, G. Klimeck, S. Rogge, S. N. Copper-smith, and M. A. Eriksson, *Reviews of Modern Physics* **85**, 961 (2013).
- [27] M. Fuechsle and M. Y. Simmons, *Single-Atom Nanoelectronics*, 61 (2013).
- [28] J. R. Petta, A. C. Johnson, J. M. Taylor, E. A. Laird, A. Yacoby, M. D. Lukin, C. M. Marcus, M. P. Hanson, and A. C. Gossard, *Science* **309**, 2180 (2005).
- [29] M. House, T. Kobayashi, B. Weber, S. Hile, T. Watson, J. van der Heijden, S. Rogge, and M. Simmons, *Nature communications* **6** (2015).
- [30] K. Petersson, C. Smith, D. Anderson, P. Atkinson, G. Jones, and D. Ritchie, *Nano letters* **10**, 2789 (2010).
- [31] T. Frey, P. Leek, M. Beck, A. Blais, T. Ihn, K. Ensslin, and A. Wallraff, *Physical Review Letters* **108**, 046807 (2012).
- [32] J. Colless, A. Mahoney, J. Hornibrook, A. Doherty, H. Lu, A. Gossard, and D. Reilly, *Physical review letters* **110**, 046805 (2013).
- [33] P. Horodecki and A. Ekert, *Physical review letters* **89**, 127902 (2002).
- [34] J. Cardy, *Physical review letters* **106**, 150404 (2011).
- [35] U. Farooq, A. Bayat, S. Mancini, and S. Bose, *Physical Review B* **91**, 134303 (2015).
- [36] M. Delbecq, T. Nakajima, P. Stano, T. Otsuka, S. Amaha, J. Yoneda, K. Takeda, G. Allison, A. Ludwig, A. Wieck, *et al.*, *Physical review letters* **116**, 046802 (2016).
- [37] R. Puddy, L. Smith, H. Al-Taie, C. Chong, I. Farrer, J. Griffiths, D. Ritchie, M. Kelly, M. Pepper, and C. Smith, *Applied Physics Letters* **107**, 143501 (2015).
- [38] E. S. Sørensen, M.-S. Chang, N. Laflorencie, and I. Affleck, *Journal of Statistical Mechanics: Theory and Experiment* **2007**, P08003 (2007).
- [39] J. Xavier and F. C. Alcaraz, *Physical Review B* **85**, 024418 (2012).
- [40] I. Affleck, *Quantum impurity problems in condensed matter physics* (Oxford University Press, 2008).
- [41] A. Bayat, P. Sodano, and S. Bose, *Physical Review B* **81**, 064429 (2010).
- [42] H. Li and F. D. M. Haldane, *Physical review letters* **101**, 010504 (2008).
- [43] G. De Chiara, L. Lepori, M. Lewenstein, and A. Sanpera, *Physical review letters* **109**, 237208 (2012).
- [44] A. Bayat, H. Johannesson, S. Bose, and P. Sodano, *Nature communications* **5**, 3784 (2014).
- [45] T. L. Curtright and D. B. Fairlie, arXiv preprint arXiv:1212.6972 (2012).
- [46] I. Devetak and A. Winter, in *Proceedings of the Royal Society of London A: Mathematical, Physical and Engineering Sciences*, Vol. 461 (The Royal Society, 2005) pp. 207–235.
- [47] H. Ollivier and W. H. Zurek, *Physical review letters* **88**, 017901 (2001).
- [48] F. F. Fanchini, M. F. Cornelio, M. C. de Oliveira, and A. O. Caldeira, *Physical Review A* **84**, 012313 (2011).
- [49] C. De Nobili, A. Coser, and E. Tonni, *Journal of Statistical Mechanics: Theory and Experiment* **2015**, P06021 (2015).
- [50] K. Życzkowski, *Open Systems & Information Dynamics* **10**, 297 (2003).
- [51] J. C. Getelina, F. C. Alcaraz, and J. A. Hoyos, *Physical Review B* **93**, 045136 (2016).